JACS
JOURNAL OF THE AMERICAN CHEMICAL SOCIETY

Article

pubs.acs.org/JACS

Effect of the Dielectric Constant of the Surrounding Medium and the Substrate on the Surface Plasmon Resonance Spectrum and Sensitivity Factors of Highly Symmetric Systems: Silver Nanocubes

Mahmoud A. Mahmoud,[†] Maysamreza Chamanzar,[‡] Ali Adibi,[‡] and Mostafa A. El-Sayed*[,†]

[†]Laser Dynamics Laboratory, School of Chemistry and Biochemistry, and [‡]School of Electrical and Computer Engineering, Georgia Institute of Technology, Atlanta, Georgia 30332-0400, United States

Supporting Information

ABSTRACT: Silver nanocubes (AgNCs), 60 nm, have four extinction surface plasmon resonance (SPR) peaks. The finite difference time domain (FDTD) simulation method is used to assign the absorption and scattering peaks and also to calculate the plasmon field intensity for AgNCs. Because AgNCs have a highly symmetric cubic shape, there is a uniform distribution of the plasmon field around them, and they are thus sensitive to asymmetric dielectric perturbations. When the dielectric medium around a nanoparticle is changed anisotropically, either by placing the particle on a substrate or by coating it asymmetrically with a solvent, the plasmon field is distorted, and the plasmonic absorption and scattering spectra could shift differently. For the 60 nm AgNC, we found that the scattering resonance peak shifted more than the absorption peak. This changes the extinction bandwidth of these overlapping absorption and scattering bands, and consequently the figure of merit of the nanoparticle, as a localized SPR sensor, no longer has a constant value.

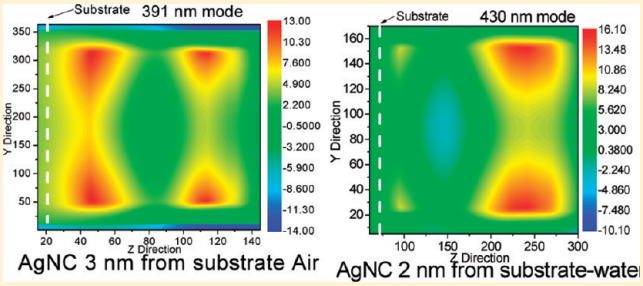

INTRODUCTION

Plasmonic nanoparticles, such as gold and silver nanoparticles, have attracted the attention of many researchers in the last couple of decades.[1,2] This great interest in plasmonic nanoparticles comes from their wide variety of optical and biological applications.[3−7] These applications are based on using their SPR spectrum and the plasmonic field.[8−10] The attractive properties of plasmonic nanoparticles have encouraged the synthesis and study of the properties of nanoparticles of different shapes and sizes to obtain nanoparticles with high plasmon fields and also to extend the SPR peak positions to the visible and the near-infrared (NIR) wavelengths.[11−13] Although the synthesis of nanoparticles by colloidal chemical methods offers good control over their shape and size and the crystal structure, it does not give any control over the separation distance between the nanoparticles in solution. Therefore, coupling between the plasmon fields of neighboring nanoparticles may take place and change the plasmon field distribution and intensity, resulting in a shift in the SPR peak position. This change in the SPR peak position limits the application of plasmonic nanoparticles in nanosensing.[7,14] Loading the colloidal plasmonic nanoparticles onto a support[15] or assembling them on a substrate is a practical solution. Recently, the Langmuir−Blodgett technique[16−18] has been used successfully to assemble plasmonic nanoparticles of different shapes and sizes into a monolayer on the surfaces of different substrates. Electron beam lithography and nanosphere lithography techniques[19] have also been used to manufacture nanoparticles on the surface of a substrate. These lithographic techniques have been successful in manufacturing different shapes and sizes of nanoparticles on a substrate with well-controlled separation distances between the particles. However, these methods have some limitations: they are not cost-effective; they are limited to nanoparticle shapes with flat top surfaces; and using these methods, only polycrystalline nanoparticles can be produced. In addition, inhomogeneity can arise due to electron beam shadowing effects, especially for nanoparticles with sharp corners or edges. Thus, as compared to colloidal synthetic methods, it is more difficult to obtain nanoparticles with sharp corners using electron beam lithography with lift-off techniques. Another parameter to consider is the separation between the nanoparticles (prepared by either a colloidal chemical method or a lithographic method) and the surface of the substrate that they are placed on. For the colloidally synthesized nanoparticles, the capping material on the surface of the nanoparticles separates the nanoparticles from the substrate.[20] For lithographic techniques, a thin layer of a transition metal (such as chromium or titanium) is usually used to bind the nanoparticles to the substrate.[21] Previous studies have shown that the substrate affects the SPR spectrum and the plasmon field of the plasmonic nanoparticles, and as the distance between the substrate and the nanoparticles

Received: January 27, 2012
Published: March 15, 2012

   dx.doi.org/10.1021/ja300901e | J. Am. Chem. Soc. 2012, 134, 6434−6442

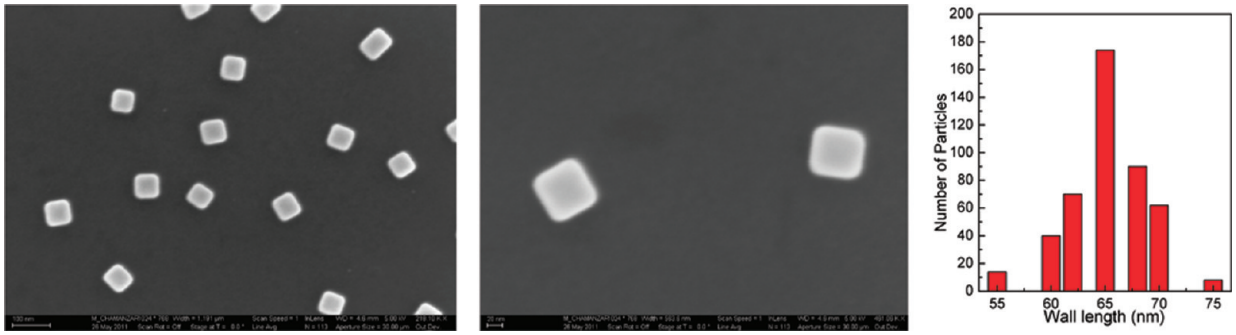

Figure 1. SEM and the particle size distribution of AgNCs with average wall length of 65 nm; the scale bar is 100 nm in the left image and 20 nm in the right image.

decreases, the plasmon field and the spectrum gets distorted.[22,23]

Silver nanocubes (AgNCs) have four SPR peaks in aqueous media, one of which is a shoulder. Discrete dipole approximation (DDA) calculations could provide an accurate assignment of the four plasmon peaks.[16] Although all of the SPR plasmon peaks of AgNCs were represented in the DDA calculated spectrum, the SPR peaks were narrower than the corresponding experimental ones. It has been reported that AgNCs assembled into a monolayer on the surface of a quartz substrate have four SPR peaks that are much narrower than those of colloidal nanoparticles and can be resolved more easily[17,24] perhaps due to smaller inhomogeneous broadening.

In this Article, we study the effect of the quartz substrate on the SPR spectral peaks and SPR plasmon field of AgNCs assembled into a Langmuir–Blodgett monolayer on the surface of a quartz substrate. The SPR spectra of AgNCs on quartz substrates were measured in several solvents with different dielectric medium constants. FDTD simulations were used to assign the SPR peaks of AgNCs as well as to monitor the effect of the substrate and the solvent on the SPR spectrum and field.

■ EXPERIMENTAL SECTION

AgNCs were prepared in ethylene glycol solvent (EG) by Xia's method[12] with some modifications.[16] In a 100 mL round-bottom flask, 70 mL of EG was stirred and heated at 140 °C for 1 h in an oil bath. After the 1 h of heating, 0.8 g of polyvinyl pyrrolidone (PVP) (molecular weight of ~55 000 g) dissolved in 10 mL of EG was added at once to the reaction mixture. The temperature of the reaction mixture then was raised gradually until it reached 155 °C. Next, 0.8 mL of 3 mM sodium sulfide in EG was added 5 min after adding PVP. Five milliliters of $AgNO_3$ (0.48 g dissolved in 10 mL of EG) was added to the reaction mixture. After the $AgNO_3$ was added, the reaction mixture was stirred until the solution became nontransparent. To clean the AgNCs from the EG solvent and excess PVP, the AgNCs solution was diluted to twice of its original volume with a water–acetone mixture and centrifuged at 13 000 rpm for 5 min. The AgNCs were precipitated down and redispersed in 50 mL of deionized water (DI).

To prepare the AgNCs for Langmuir–Blodgett (LB) deposition, the solution was centrifuged at 13 000 rpm for 5 min, and the AgNCs precipitate was dispersed in 10 mL of chloroform. The Langmuir–Blodgett monolayer was prepared using a Nima 611D trough; the sublayer of the trough was DI water. The surface pressure was measured with a paper Wilhelmy plate attached to a D1L-75 model pressure sensor. An aliquot of 2 mL of AgNCs dispersed in chloroform was sprayed over the water surface, and the monolayer was left for 10 min to dry. The LB film was transferred to quartz and silicon substrates (cleaned with piranha solution 30% H_2O_2+70% H_2SO_4 volume ratio) by the vertical dipping method at a surface pressure of 0 mN/m. The Ocean Optics HR4000Cg-UV–NIR was used for UV–vis absorption measurements. The optical measurements for the AgNCs monolayer were carried out by fixing the substrates vertically inside a quartz cuvette. A Zeiss Ultra60 scanning electron microscope (SEM) was used for SEM imaging.

■ RESULTS AND DISCUSSION

Characterization of AgNCs Monolayers. Langmuir–Blodgett is a valuable technique for assembling colloidal nanoparticles into monolayers. However, the interparticle separation distance between the nanoparticles cannot be controlled[20,25] to be an exact value. Figure 1 shows the SEM image of the Langmuir–Blodgett monolayer of AgNCs assembled on the surface of a silicon wafer substrate as well as the particle size distribution of AgNCs. For more accurate calculation of the particle size of the AgNCs, a statistical calculation is carried out for 450 particles present in two SEM images (see Figure S1). From the statistical size distribution, it can be seen that the largest frequency corresponds to the wall length of 65 nm. Therefore, we can assume that the average wall length of the nanoparticles is 65 nm, and the broadening due to the size variation does not affect the results much. To decrease the effect of the SPR field coupling between different nanoparticles, we have made the separation distance between neighboring nanoparticles more than 100 nm.

Assignment of the Observed Extinction Spectra of AgNC Monolayers. The shape, size, and the dielectric constant of the medium surrounding the plasmonic nanoparticles are responsible for the observed SPR extinction spectrum, the plasmon field profile, and the intensity. For nanoparticles with high symmetry, such as cubes or spheres, breaking the symmetry by changing the shape or the surrounding of the plasmonic nanoparticles could change the SPR resonance features.[22,26] When the plasmonic nanoparticles are excited at their SPR resonance wavelengths, the surface plasmon resonances of the conduction band electrons generate strong electromagnetic fields.[2,27,28] This leads to an enhancement in the radiative and nonradiative electronic properties of the nanoparticles themselves, as well as of those nearby electronic systems. The near-field effects enhance the absorption and scattering processes by amplifying the electromagnetic fields of the resonant exciting light. However, the amplified SPR electromagnetic extinction spectrum consists of an unequal contribution of absorption and scattering yields. For a single plasmonic nanoparticle, its shape, size, material, and dielectric constant of the surrounding medium determine the SPR peak position, the ratio between the absorption and scattering yields, and the plasmon field intensity and distribution. Plasmonic nanoparticles are used in many applications such as surface enhanced Raman spectroscopy

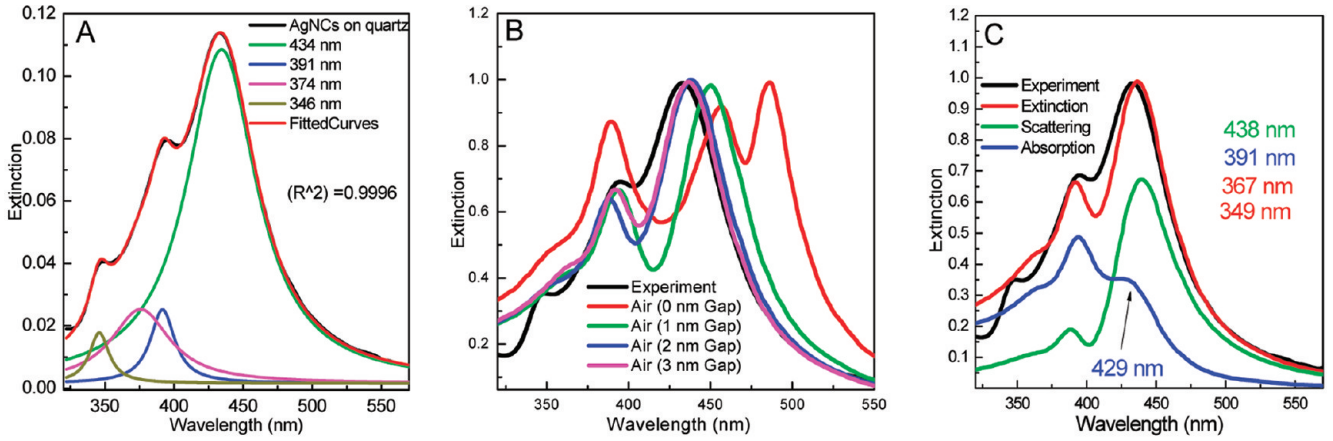

Figure 2. (A) Experimental SPR spectrum of 65 nm AgNCs assembled onto a LB monolayer on the surface of a quartz substrate; the spectrum was deconvoluted into four peaks. The black spectrum is the experimentally observed SPR of AgNCs, while the fitted curve is in red. (B) The SPR extinction spectrum of 65 nm AgNCs calculated with FDTD; the simulations carried out for AgNCs at different separation distances (0, 1, 2, and 3 nm) from a quartz substrate. (C) The SPR spectrum of 65 nm AgNCs (extinction, scattering, and absorption) calculated with FDTD at a 3 nm separation distance from a quartz substrate. The black colored spectrum is the experimental SPR spectrum normalized to unity.

(SERS),[17] fluorescence enhancement,[24] biological sensing,[29] and photodynamic thermal therapy.[30] In some applications, strong absorption is desired, while other applications use their strong scattering properties. To obtain the optimum efficiency in such applications, the optical properties of the plasmonic nanoparticles need to be carefully examined. In the case of small size nanoparticles, the absorption and scattering bands are coincident, and the absorption contributes to the extinction spectrum more strongly than the scattering. As the nanoparticle size increases, the scattering becomes predominant, and its spectrum shifts away from the absorption.[31] Figure 2A shows the SPR spectrum of AgNCs assembled on a surface of a quartz substrate; some of the peaks show strong overlap. Although three distinct peaks can be easily distinguished, there is a weak shoulder at 391 nm. This shoulder becomes more profound as the size of the particle is increased; for example, for an AgNC with a size of 80 nm, this shoulder is better resolved, as shown in Figure S2. To resolve these peaks, we have deconvoluted the spectrum into four peaks at 434, 391, 374, and 346 nm, with a very good fit (R^2 = 0.9996).

To assign the absorption and scattering contributions to the measured extinction spectrum, we have used the FDTD technique to simulate the electromagnetic properties of the AgNCs. The permittivity of silver is modeled using the empirical results of Johnson and Christy.[32] In each case, the scattered and total fields are computed, and then the absorption and scattering cross sections are calculated as functions of frequency by performing a discrete Fourier transform (DFT) on the time domain results. The simulation domain is finely meshed with a mesh size of 1 nm so that the convergence of the results and the accuracy of the computed fields are confirmed.

During the synthesis of AgNCs, PVP polymer was used as a capping agent. Although the surface of the nanoparticles was cleaned well, some PVP chains still remain attached to the surface of some of the AgNC nanoparticles. The PVP chains determine the distance between the AgNCs and the surface of the substrate. Yang's group calculated the separation distance between two neighboring 150 nm AgNCs within an aggregated dimer and found that the separation distance is ~2 nm.[18,33] Recently, the separation distance between two gold nanocages capped with PVP was found to be ~2 nm.[20] Schatz's group found from their calculation of 30 nm AgNCs on the surface of a substrate at different separation distances that as the distance between the substrate and the nanoparticles increases, the SPR peak positions change.[22] To determine the actual separation distance between the substrate and the AgNC in the LB monolayer film, we have carried out FDTD simulations of AgNCs on substrate at different separation distances and have compared each SPR spectrum with the experimental spectrum. Figure 2B shows the FDTD calculations of AgNCs on a quartz substrate at separation distances of 0, 1, 2, and 3 nm. Although the calculated SPR spectra at 1, 2, and 3 nm separation distances have spectral shapes similar to the experimentally measured spectrum, the 3 nm distance best matches the experimental SPR spectrum. The calculated SPR spectrum of AgNCs directly placed on the surface of a quartz substrate with no spacer differs significantly from the experimental spectrum as well as from the calculations at 1, 2, and 3 nm distances. Specifically, the most intense peak at lower energy splits into two peaks. This extra peak for zero separation distance could be a result of a Fano resonance[23]or due to splitting of the most intense plasmon peak resulting from the effective symmetry reduction.[22] Figure 2C shows the FDTD simulation of 65 nm AgNCs at 3 nm distance from a quartz substrate. On the basis of our FDTD calculations, AgNCs have four extinction peaks at 438, 392, 367, and 349 nm. In the SPR peak around 438 nm, the scattering and absorption are separated; the SPR scattering is at 438 nm, while the absorption is at 429 nm. The contribution of the absorption in this peak is small as compared to the scattering. The observed peak at 391 nm can result from the overlap of both scattering peak at 388 nm and absorption at 393 nm. The separation between the scattering and absorption peaks is not large, and the absorption contributes more to this SPR peak than to the 435 nm peak. Moreover, the scattering peak of the 393 nm extinction peak appears at a wavelength shorter than the absorption peak. For peaks at 367 and 349 nm, the absorption contributes more than the scattering. In comparing the theoretical and experimental results, all of the experimental SPR peaks are predicted by the simulation results. Therefore, if scattering is measured for the AgNCs, only the two SPR peaks corresponding to scattering at 434 and 391 nm should be observed as was indeed reported before by Sherry et al.[22] They measured the dark-field scattering for a single 30 nm AgNC assembled on the surface of quartz substrate by drop

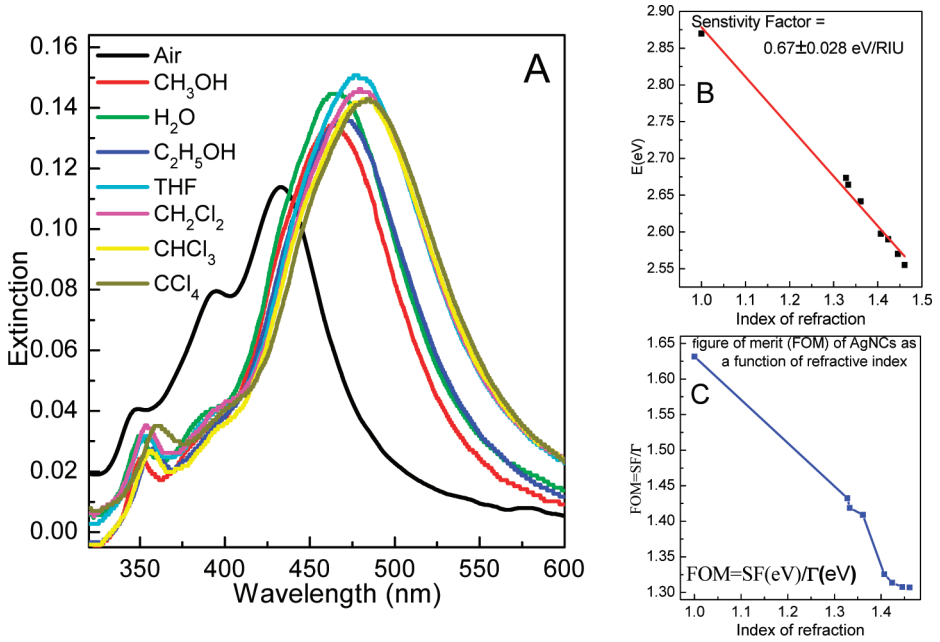

Figure 3. (A) SPR spectra of AgNCs assembled on the surface of a quartz substrate measured in the different solvent and in air. (B) Linear relationship between the SPR position of the strong band and refractive index of the surrounding medium. (C) The relationship between the FOM of AgNCs and the refractive index of the solvent.

casting. Two sharp scattering peaks are observed for AgNCs in the water environment.

Sensitivity Factor of AgNCs versus Figure of Merit. The sensitivity factor (SF) is one of the figures of merits (FOM) for plasmonic nanoparticles in sensing.[19,34,35] It is defined as the amount of shift in the SPR peak position in electron volts (eV) or nanometers per unit change in the refractive index (RIU) of the surrounding medium (SF is expressed in the unit of eV/RIU or nm/RIU). The SPR peak position is sensitive to the dielectric constant of the surrounding environment (bulk sensitivity) as well as the type of molecules bound to its surface (surface sensitivity).[10,36] A red-shift in the SPR peak position is observed as the refractive index of the surrounding medium increases.[6,37,38] The value of the sensitivity factor depends on the shape, size, and type of the plasmonic nanoparticle.[9,39]

The detection limit is an important figure of merit in optical sensing. The detection limit is defined as the minimum amount of analyte that can be detected. It depends on the sensitivity as well as the resolution of the detection mechanism in locating a resonance peak position. The resolution thus depends on the sharpness of the SPR peak as measured by the full width at half-maximum (FWHM) of the resonance band, as well as the signal-to-noise ratio.[40] FOM can be defined for the nanoparticle sensors as the ratio of the SF (in eV/RIU units) to the FWHM of the SPR resonance in eV units.[40] The detection limit is inversely proportional to the value of FOM.

Figure 3A shows the SPR spectra of an AgNCs monolayer assembled on the surface of a quartz substrate and measured in air and in different solvents (e.g., methanol, water, ethanol, tetrahydrofuran (THF), dichloromethane, chloroform, and carbon tetrachloride). The SPR spectra of AgNCs in all solvents have three well-resolved peaks in addition to the shoulder. The SPR peak position of the AgNCs is found to red-shift as the surrounding refractive index of the solvent increases. Moreover, the FWHM of the most intense resonance peak was found to increase as the refractive index of the surrounding medium increased. The SPR spectral peak position of the most intense resonance peak of the AgNCs, measured in different solvents, is plotted in Figure 3B versus the refractive index of the surrounding solvent. The SF of the AgNCs is the slope of the linear fit to the SPR peak position (in eV units) in different solvents versus the reflective index of each solvent. The SF was found to be 0.67 ± 0.028 eV/RIU or 113 ± 5 nm/RIU. Previously, we reported[13] the highest experimentally reported SF value of 620 ± 15 nm/RIU, which was measured for gold nanoframes of 51 nm wall length and 10 nm wall thickness. The smallest experimentally reported SF value is 44 nm/RIU, reported for gold nanospheres.[41] It is also found that the SF is large for cavity type particles of the same shape due to the coupling between their outer and inner surface Plasmon fields.[13] Although the SF of AgNCs is not large as compared to other shapes of plasmonic nanoparticles, their SPR spectral bandwidth is narrow enough to make their FOM sufficiently large.

To examine the stability of the AgNCs monolayer and the consistency of the SPR measurement in different solvents, the AgNCs monolayer on a quartz substrate was left to dry from each solvent, and the SPR spectrum was compared to that taken in air (see Figure S3). The SPR spectra for the AgNCs before and after the optical measurements in the solvents are superimposable, which suggests that the measurement is reversible. This is attributed to the stability of the AgNC monolayers during the measurements, and the change in the SPR spectrum in the solvents is due to the change in the refractive index of the surrounding medium.

Figure 3C shows the relationship between the FOM and the refractive index. Figure 3B shows the FWHM of the strongest band in the SPR spectrum of AgNCs in each solvent. It can be seen from Figure 3C that the FOM is not constant, and it decreases as the refractive index of the solvent is increased. The reason is that the FWHM increases as the refractive index is increased, while the SF is constant. The conclusion here is that, although the value of the FOM determines the accuracy of the

dx.doi.org/10.1021/ja300901e | J. Am. Chem. Soc. 2012, 134, 6434−6442

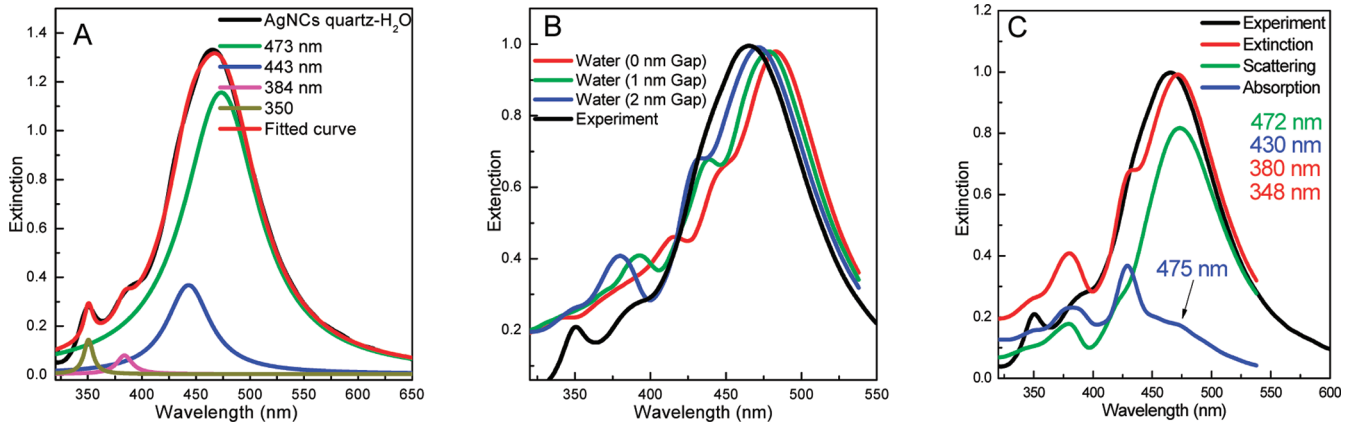

Figure 4. (A) The SPR spectrum of AgNCs assembled into a monolayer on the surface of a quartz substrate measured in water surrounding medium (black): this spectrum was deconvoluted into four peaks. The fitted curve appears in red. (B) FDTD calculation of 65 nm AgNCs on the surface of quartz substrate at different separation distances (0, 1, 2 nm); the black spectrum shows the experimental data. (C) The SPR spectrum of 65 nm AgNCs (extinction, scattering, and absorption) calculated with FDTD at 2 nm separation distance from a quartz substrate and surrounded with water. The black curve is the normalized experimental SPR spectrum normalized to unity.

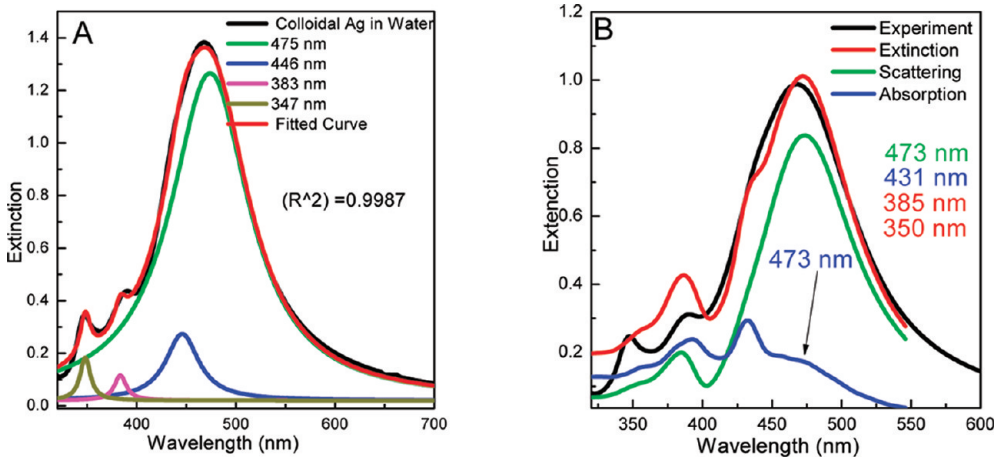

Figure 5. (A) The SPR spectra of colloidal AgNCs in water. (B) FDTD results for the SPR extinction cross section (red curve), scattering (green curve), and absorption (blue curve) for 65 nm colloidal AgNCs dispersed in water.

sensing measurement with plasmonic nanoparticles, the FOM changes as the refractive index of the surrounding medium changes, and this has to be considered in the calibration of the plasmonic nanosensors. However, in considering different nanoparticles for sensing, the FOM is best for those that have a sharp SPR spectrum and for particles whose scattering and absorption band characteristics (wavelength and bandwidth) change similarly.

SPR Peak Broadening with Increasing the Dielectric Constant of the Surrounding Medium. The SPR spectrum of nanoparticles consists of unequal contributions of the SPR absorption and the SPR scattering. For some plasmonic nanoparticles, the absorption and scattering SPR peaks may coincide, and for some shapes and sizes, they may not. Stated in another manner, the extinction spectrum has overlapping bands due to the absorption and scattering. For the dielectric constant in this present system, the degree of overlapping and the amount of broadening will be affected by changing the solvent. The important issue is whether the change of the refractive index of the medium surrounding the nanoparticles causes the same amount of shift in the scattering and absorption SPR peaks. Figure 4A shows the measured SPR extinction spectrum of a monolayer of AgNCs immobilized on the surface of a quartz substrate and submersed in water. The SPR spectrum has three well-resolved peaks in addition to a shoulder at 446 nm. This SPR spectrum is deconvoluted into four peaks: 473, 443, 384, and 350 nm. As previously discussed, the separation distance between the substrate and the AgNCs has a profound effect on the shape of the SPR peaks and was found to be 3 nm for the AgNCs, and the quartz substrate was 3 nm, when surrounded with air. However, when we carried out the FDTD calculations for the AgNCs on the surface of quartz substrate at a separation distance of 3 nm and surrounded with water, the shape of the SPR spectrum was not similar to the experimental one. To determine the actual separation distance, we carried out FDTD simulations of 65 nm AgNCs dispersed in water and AgNCs placed at 0, 1, and 2 nm away from a quartz substrate and surrounded with water (see Figure 4B). The refractive index of water is assumed to be $n = 1.333$, where the dispersion of water throughout the bandwidth of the nanoparticle resonance is neglected. Figure 4B shows the SPR spectrum of AgNCs placed on the surface of a quartz substrate at different separation distances (0, 1, and 2 nm) calculated by the FDTD technique method. The simulated spectrum at the 2 nm separation distance matches well with the experimental result. Figure 4 C shows the results of the FDTD calculation of 65 nm

dx.doi.org/10.1021/ja300901e | J. Am. Chem. Soc. 2012, 134, 6434−6442

AgNCs placed at a separation distance of 2 nm from the surface of a quartz substrate and surrounded with water. The scattering and the absorption cross section of the AgNCs obtained from the FDTD analysis in Figure 4C show that the main resonance peak at 473 nm arises mostly from the scattering of the nanoparticle, while the peak at 443 nm arises from the absorption. The resonance peak at 384 nm arises from both absorption and scattering by the nanoparticle. It should be noted that the small discrepancies between the simulation and the experimental results can be attributed to a number of different causes. First, the dimensions of the AgNCs as measured from the scanning electron micrographs (SEMs) are accurate only within ±2 nm. Also, the material properties that we have used in the simulations might be slightly different from those of the actual sample. Both of these effects can contribute to the discrepancies between the simulation and the experimental results. The interesting observation is that, unlike the peak at 434 nm for AgNCs surrounded with air, the scattering and the absorption peaks at 473 nm are only separated by 2 nm, and the scattering peak is much broader. The SPR peaks of AgNCs shifted from 434, 391, 374, and 346 nm in the case of air-quartz to 473, 443, 384, and 350 nm, respectively, in the water-quartz medium. The peak at 434 nm is shifted by 39 to 473 nm, while the peak at 391 nm shifts by 52 to 443 nm.

The dielectric constant of the surrounding medium is responsible for the change in the SPR peak positions of the isolated plasmonic nanoparticles. However, the dielectric constant of the medium can be changed by either a ligand that binds to the nanoparticle, the polymer matrix, or the surrounding solvent. Yet if the nanoparticle is placed on a surface of a substrate or combined with another nanoparticle in a dimer or aggregate, the SPR peak position will change. In this section, we have studied the effect of changing the refractive index of the surrounding medium, while the AgNCs are placed on the substrate. Figures 5A and 4A, respectively, show the SPR spectrum of colloidal AgNCs in water and that of AgNCs placed on the surface of a quartz substrate and surrounded with water. To monitor the effect of the substrate on the SPR spectrum of AgNCs surrounded with water, we compared the SPR peaks of the colloidal AgNCs in water solution and the corresponding ones of an AgNC monolayer assembled on a quartz substrate with surrounding aqueous medium. A small red-shift was observed in the case of the colloidal nanoparticles in water. However, the colloidal AgNCs have six faces exposed to the surrounding water, while the monolayer assembly on the quartz substrate has only five faces exposed to water if it is in contact with the surface of the substrate. The sixth face of the AgNC is touching the quartz substrate surface. The dielectric constant of quartz is higher than that of water. Therefore, the SPR peak positions of AgNCs placed on the quartz substrate are expected to appear at longer wavelengths as compared to the one in colloidal solution. However, the opposite is observed. This result supports what was concluded in the last section from the results shown in Figure 4, regarding the AgNCs at a 2 nm separation distance from the quartz substrate. Another observation is that the peak at 383 nm is much broader when the AgNCs is placed on the quartz substrate and surrounded with water than for the colloidal AgNCs. However, the FWHM of the most intense peak of AgNCs placed on the surface of a quartz substrate is narrower than that for colloidal AgNCs. To understand the reason for this, we carried out FDTD calculations for the AgNCs in water. It was proved that the peak at 380 nm arises from both absorption and scattering (as shown in Figures 4C and 5B). The shift of the SPR absorption peak from the scattering peak is larger in case of AgNC when placed on the surface of quartz substrate than for the colloidal AgNC. Furthermore, the absorption peak in colloidal AgNCs is much sharper than that of AgNC on a substrate. The reason for the peak at 473 nm being much broader in the case of colloidal AgNCs than the main SPR peak of the AgNCs on the substrate could be that the scattering peak is much broader in the case of AgNCs colloidal due to more inhomogeneous broadening.

The deconvolution of the SPR spectral peaks of AgNCs dissolved in chloroform solvent shows that, similar to AgNCs in water, it has four peaks at 496, 455, 387, and 350 nm, while for AgNCs placed on a quartz substrate and surrounded with chloroform the peaks are at 487, 445, 391, and 354 nm (see Figure S4). Although the shape of the SPR spectrum of AgNCs surrounded with chloroform is similar to that surrounded with water medium, three differences were observed: (1) The most intense peak is much broader; (2) all of the peaks were red-shifted after changing the surrounding medium from water to chloroform; and (3) large red-shifts were observed in the SPR peaks of AgNC dispersed in chloroform as compared to AgNCs on quartz and surrounded with chloroform. On the basis of our former assignments of the AgNCs SPR peaks, the SPR peak of AgNCs placed on the quartz substrate at 487 nm arises from scattering, while the peak at 445 nm arises from absorption. The SPR peaks at 434 and 391 nm for AgNCs placed on the surface of a quartz substrate and surrounded with air are red-shifted to 487 and 445 nm, respectively, for the AgNC on quartz and surrounded with chloroform. As a comparison, we can see that the SPR peak of AgNCs placed on the quartz substrate at the resonance wavelength of 391 nm is red-shifted by 52 nm when the surrounding medium is changed from air to water and by 54 nm when the surrounding medium is changed to chloroform. On the other hand, the peak at 434 nm is shifted by 39 nm (for surrounding water medium) and 52 nm (for surrounding chloroform medium). The difference in the red-shift in absorption and scattering peaks by increasing the dielectric constant of the medium from water to chloroform causes an increase in the FWHM of the more intense peak of the AgNCs placed on the surface of the quartz substrate.

FDTD Calculation for the Field Intensity of Colloidal AgNCs and AgNCs on Substrate. The experimental and theoretical calculations showed that AgNCs placed on the surface of a quartz substrate (either surrounded with air or a solvent) do not touch the substrate, and there is always a 2−3 nm gap between the substrate and the AgNCs. There are some observations that require further investigation: (1) when the refractive index of the medium around the AgNCs on the surface of a quartz substrate is increased, the main SPR peak becomes broader; and (2) the peak at ∼380 nm, arising from both the absorption and scattering of the AgNCs, becomes broader when AgNCs are placed on the surface of a quartz substrate (surrounded with a solvent) as compared to that of the colloidal AgNCs. However, the opposite was observed for the FWHM of the sharp SPR peak of AgNCs. Therefore, the substrate still has an effect on the SPR even at a separation distance of 2−3 nm. To study the effect of the substrate on the resonances of plasmonic nanoparticles, we have performed FDTD analysis of a 65 nm AgNC placed on the surface of a quartz substrate in air. The dispersion of quartz over the entire bandwidth of the plasmonic resonance line shape is taken into

dx.doi.org/10.1021/ja300901e | J. Am. Chem. Soc. 2012, 134, 6434−6442

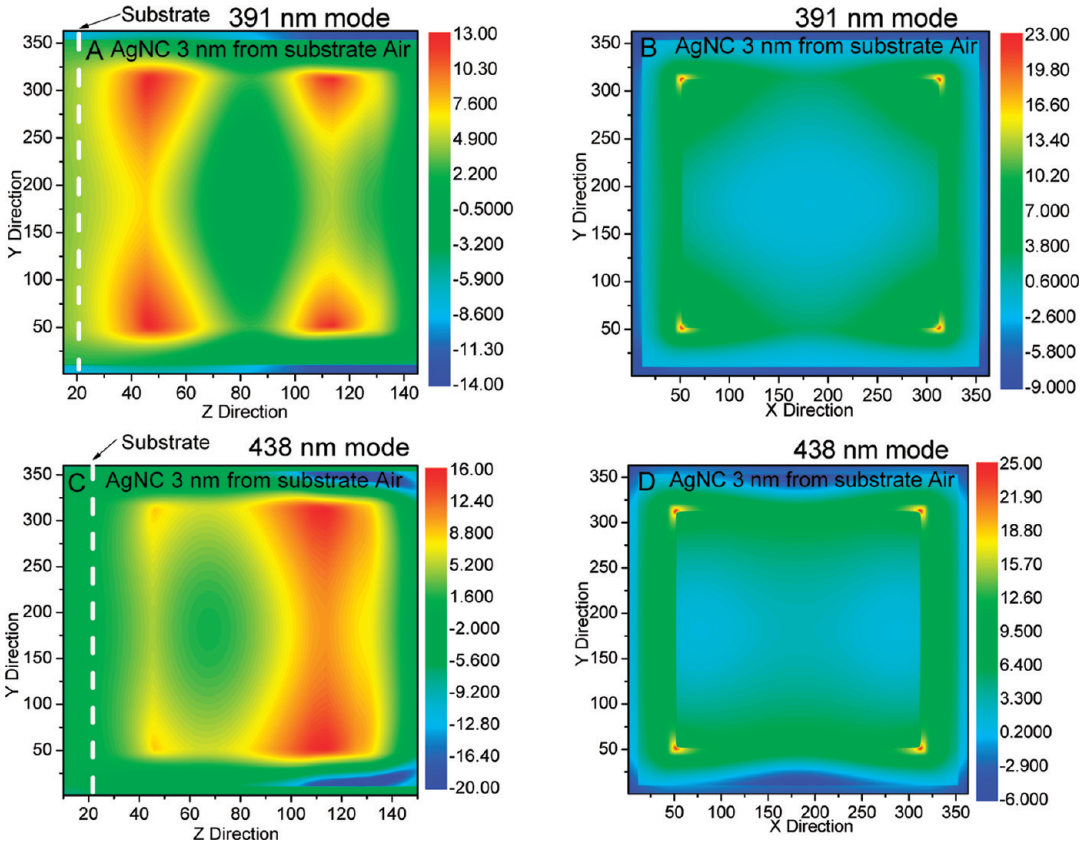

Figure 6. The field intensity in log scale ($\log(|E|^2)$) of 65 nm AgNCs at a 3 nm distances, from a quartz substrate calculated with the FDTD technique at different SPR plasmon modes. (A,C) The field intensity contour in the center of the AgNC and perpendicular to the surface of the quartz substrate, for 391 nm and 438 modes, respectively. (B,D) The field intensity contour of the AgNC calculated parallel to the surface of a quartz substrate, at 391 nm and 438 modes, respectively.

account. Figure 6 shows the FDTD calculation results of the field intensity of 65 nm AgNCs, in log scale ($\log(|E|^2)$), placed on the surface of a quartz substrate at a separation distance of 3 nm. The field profiles are calculated at different SPR resonant modes perpendicular to and parallel with the surface of the substrate. The field intensity contour perpendicular to the surface of the quartz substrate for the 391 nm resonant mode has high intensity close to the surface of the substrate (see Figure 6A), while the field intensity of the 438 nm resonance mode has a high field intensity distribution far from the surface of substrate, on the surface of the AgNC (see Figure 6C). The calculation for the plasmon field intensity in a plane parallel to the substrate and passing through the middle of the particle has high intensity at the corners of the AgNC in both 391 and 438 nm modes as shown in Figure 6B and D.

The experimental results and the FDTD calculations show four resonance peaks for AgNCs placed 2 nm from the surface of the quartz substrate when the surrounding medium is water (Figure 4C). In this FDTD simulation, similar to all previous simulations, the gap region is meshed with a mesh size of 0.2 nm to ensure accurate convergence of the results. The plasmon field intensity is calculated for the three SPR modes parallel and perpendicular to the surface of the substrate. Figure 7A, C, and E shows the perpendicular plasmon field for AgNCs placed 2 nm from a quartz substrate and surrounded with water. For the 385 nm resonance mode, the field intensitieson the top surface of the nanoparticle and also on the bottom close to the substrate are almost the same. This could be the reason for the broadening of the peak at 385 nm of the AgNC placed on the substrate, because the field intensity of the AgNCs in the colloidal water medium has uniform distribution (see Figure S5). For the AgNCs placed on the surface of a quartz substrate, when the surrounding medium is changed from air to water, the resonance wavelength is shifted from 391 to 430 nm, and the field intensity distribution is changed. In the case of the surrounding air, the field intensity near the quartz substrate is less intense than the field intensity far from the substrate on the surface of the AgNC. However, in the case of water surrounding, the field intensity on the surface of the AgNC near the quartz substrate is comparable to that on the surface of the AgNC far from the substrate. The field intensity for the 472 nm mode of the AgNCs in the water−quartz system has a similar distribution to the 438 nm mode of the AgNCs in the air−quartz system, and this mode is responsible for the broadening of the FWHM of the SPR of the AgNC and therefore change of the FOM value. Finally, the plasmon field intensity distribution parallel to the substrate is comparable for the three different plasmon modes.

CONCLUSIONS

A number of observations and conclusions have been made regarding the plasmonic spectra of highly symmetric and relatively large nanoparticles such as silver nanocubes (AgNCs): (1) The scattering and absorption band frequencies can shift differently in different dielectric media. (2) This causes band broadening by amounts that depend on the solvent dielectric constant making the figure of merit not have a constant value. (3) The effect of the substrate is stronger due to

dx.doi.org/10.1021/ja300901e | J. Am. Chem. Soc. 2012, 134, 6434−6442

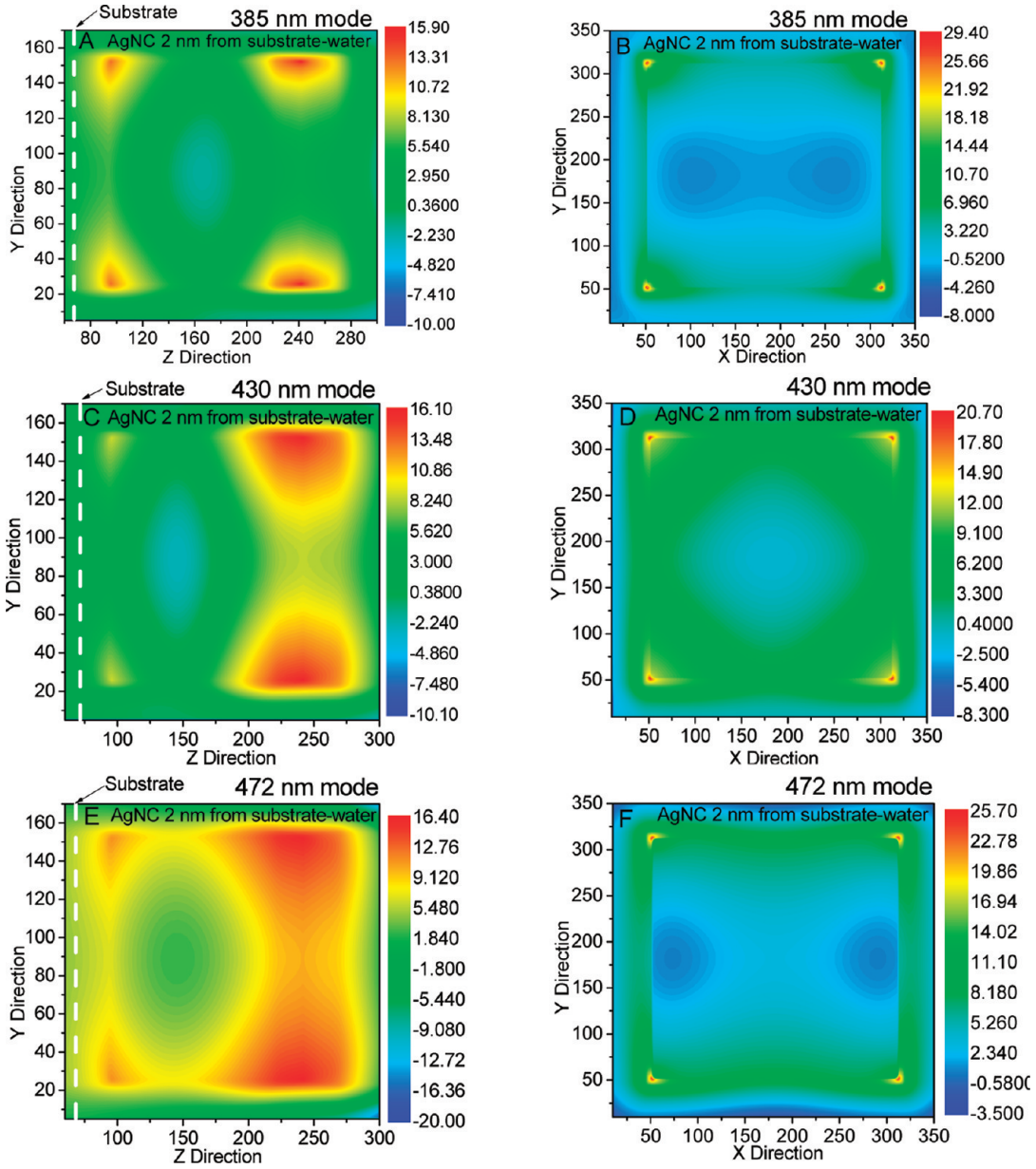

Figure 7. The field intensity in log scale ($\log(|E|^2)$) of a 65 nm AgNC at a distance of 2 nm from the surface of a quartz substrate and surrounded with water, calculated using the FDTD technique at different SPR plasmon modes. (A,C,E) The field intensity contour in the center of the AgNC and perpendicular to the surface of the quartz substrate, for 385, 430, and 472 nm, respectively. (B,D,F) The field intensity contour of AgNC calculated parallel to the surface of the quartz substrate, at 385, 430, and 472 nm modes, respectively.

the splitting of the degeneracies present in highly symmetric systems in systems, especially when the particle is not strongly shielded by thick or polar capping material. (4) This effect is sensitive to the solvent as it changes the dielectric constant of the surrounding medium, and consequently the amount of scattering and absorption peak shift. Some of these experimental conclusions are supported by theoretical computations.

■ ASSOCIATED CONTENT

Supporting Information

SEM image of large numbers of AgNCs (Figure S1). SPR spectrum of 80 nm AgNCs placed on a quartz substrate (Figure S2). SPR spectra of AgNCs before and after exposure to the solvents (Figure S3). SPR spectra of AgNCs assembled into monolayer on the surface of quartz substrate measured in chloroform solution and colloidal AgNCs in chloroform solvent (Figure S4). Results of the FDTD calculation of the SPR spectrum of 65 nm colloidal AgNCs dispersed in water solution (Figure S5). This material is available free of charge via the Internet at http://pubs.acs.org.

■ AUTHOR INFORMATION

Corresponding Author

melsayed@gatech.edu

Notes

The authors declare no competing financial interest.

■ ACKNOWLEDGMENTS

This work was supported by the Defense Advanced Research Projects Agency (DARPA) under Contract No. HR 0011-10-1-0075.

■ REFERENCES

(1) Kreibig, U.; Vollmer, M. *Optical Properties of Metal Clusters*; Springer Series in Materials Science 25; Springer: New York, 1995.
(2) Link, S.; El-Sayed, M. A. *Int. Rev. Phys. Chem.* **2000**, *19*, 409.
(3) Moskovits, M. *J. Chem. Phys.* **1978**, *69*, 4159.
(4) Albrecht, M. G.; Creighton, J. A. *J. Am. Chem. Soc.* **1977**, *99*, 5215.
(5) Reinhard, B. M.; Siu, M.; Agarwal, H.; Alivisatos, A. P.; Liphardt, J. *Nano Lett.* **2005**, *5*, 2246.
(6) Storhoff, J. J.; Lazarides, A. A.; Mucic, R. C.; Mirkin, C. A.; Letsinger, R. L.; Schatz, G. C. *J. Am. Chem. Soc.* **2000**, *122*, 4640.
(7) Mahmoud, M. A.; El-Sayed, M. A. *Nano Lett.* **2009**, *9*, 3025.
(8) Jin, R.; Cao, Y.; Mirkin, C. A.; Kelly, K. L.; Schatz, G. C.; Zheng, J. G. *Science* **2001**, *294*, 1901.
(9) Malinsky, M. D.; Kelly, K. L.; Schatz, G. C.; Van Duyne, R. P. *J. Am. Chem. Soc.* **2001**, *123*, 1471.
(10) El-Sayed, I. H.; Huang, X.; El-Sayed, M. A. *Nano Lett.* **2005**, *5*, 829.
(11) Nikoobakht, B.; Wang, J.; El-Sayed, M. A. *Chem. Phys. Lett.* **2002**, *366*, 17.
(12) Sun, Y. G.; Xia, Y. N. *Science* **2002**, *298*, 2176.
(13) Mahmoud, M. A.; El-Sayed, M. A. *J. Am. Chem. Soc.* **2010**, *132*, 12704.
(14) Mahmoud, M. A.; Snyder, B.; El-Sayed, M. A. *J. Phys. Chem. C* **2010**, *114*, 7436.
(15) Lee, J. H.; Mahmoud, M. A.; Sitterle, V.; Sitterle, J.; Meredith, J. C. *J. Am. Chem. Soc.* **2009**, *131*, 5048.
(16) Mahmoud, M. A.; El-Sayed, M. A. *J. Phys. Chem. C* **2008**, *112*, 14618.
(17) Mahmoud, M. A.; Tabor, C. E.; El-Sayed, M. A. *J. Phys. Chem. C* **2009**, *113*, 5493.
(18) Tao, A.; Sinsermsuksakul, P.; Yang, P. *Nat. Nanotechnol.* **2007**, *2*, 435.
(19) Jensen, T. R.; Duval, M. L.; Kelly, K. L.; Lazarides, A. A.; Schatz, G. C.; Van Duyne, R. P. *J. Phys. Chem. B* **1999**, *103*, 9846.
(20) Mahmoud, M. A.; El-Sayed, M. A. *J. Phys. Chem. C* **2011**, *115*, 12726.
(21) Tabor, C.; Murali, R.; Mahmoud, M.; El-Sayed, M. A. *J. Phys. Chem. A* **2009**, *113*, 1946.
(22) Sherry, L. J.; Chang, S.-H.; Schatz, G. C.; Van Duyne, R. P.; Wiley, B. J.; Xia, Y. *Nano Lett.* **2005**, *5*, 2034.
(23) Zhang, S. P.; Bao, K.; Halas, N. J.; Xu, H. X.; Nordlander, P. *Nano Lett.* **2011**, *11*, 1657.
(24) Mahmoud, M. A.; Poncheri, A. J.; Phillips, R. L.; El-Sayed, M. A. *J. Am. Chem. Soc.* **2010**, *132*, 2633.
(25) Mahmoud, M. A.; Qian, W.; El-Sayed, M. A. *Nano Lett.* **2011**, *11*, 3285.
(26) Knight, M. W.; Wu, Y.; Lassiter, J. B.; Nordlander, P.; Halas, N. J. *Nano Lett.* **2009**, *9*, 2188.
(27) Kerker, M. *J. Colloid Interface Sci.* **1985**, *105*, 297.
(28) Creighton, J. A.; Eadon, D. G. *J. Chem. Soc., Faraday Trans.* **1991**, *87*, 3881.
(29) Soennichsen, C.; Reinhard, B. M.; Liphardt, J.; Alivisatos, A. P. *Nat. Biotechnol.* **2005**, *23*, 741.
(30) Dickerson, E. B.; Dreaden, E. C.; Huang, X. H.; El-Sayed, I. H.; Chu, H. H.; Pushpanketh, S.; McDonald, J. F.; El-Sayed, M. A. *Cancer Lett.* **2008**, *269*, 57.
(31) Lee, K.-S.; El-Sayed, M. A. *J. Phys. Chem. B* **2006**, *110*, 19220.
(32) Johnson, P. B.; Christy, R. W. *Phys. Rev. B* **1972**, *6*, 4370.
(33) Tao, A.; Kim, F.; Hess, C.; Goldberger, J.; He, R. R.; Sun, Y. G.; Xia, Y. N.; Yang, P. D. *Nano Lett.* **2003**, *3*, 1229.
(34) Raschke, G.; Brogl, S.; Susha, A. S.; Rogach, A. L.; Klar, T. A.; Feldmann, J.; Fieres, B.; Petkov, N.; Bein, T.; Nichtl, A.; Kuerzinger, K. *Nano Lett.* **2004**, *4*, 1853.
(35) Mock, J. J.; Smith, D. R.; Schultz, S. *Nano Lett.* **2003**, *3*, 485.
(36) Haes, A. J.; Zou, S.; Schatz, G. C.; Van Duyne, R. P. *J. Phys. Chem. B* **2004**, *108*, 109.
(37) Haes, A. J.; Zou, S.; Schatz, G. C.; Van Duyne, R. P. *J. Phys. Chem. B* **2004**, *108*, 6961.
(38) Zhao, J.; Haes, A. J.; Zhang, X.; Zou, S.; Hicks, E. M.; Schatz, G. C.; Van Duyne, R. P. *Mater. Res. Soc. Symp. Proc.* **2006**, *900E*, O900.
(39) Malinsky, M. D.; Kelly, K. L.; Schatz, G. C.; Van Duyne, R. P. *J. Phys. Chem. B* **2001**, *105*, 2343.
(40) Chamanzar, M.; Soltani, M.; Momeni, B.; Yegnanarayanan, S.; Adibi, A. *Appl. Phys. B* **2010**, *101*, 263.
(41) Chen, H.; Kou, X.; Yang, Z.; Ni, W.; Wang, J. *Langmuir* **2008**, *24*, 5233.